

ASGARD: A Single-cell Guided pipeline to Aid Repurposing of Drugs

Bing He, Lana X. Garmire *

Department of Computational Medicine and Bioinformatics, University of Michigan, Ann Arbor,
MI, USA

*: Correspondence to Lana X. Garmire, Department of Computational Medicine and
Bioinformatics, North Campus Research Complex, University of Michigan, 1600 Huron Parkway,
Ann Arbor, MI 48105 USA

Telephone: (734) 615-0514

Email: lgarmire@med.umich.edu

Abstract

Intercellular heterogeneity is a major obstacle to successful personalized medicine. Single-cell RNA sequencing (scRNA-seq) technology has enabled in-depth analysis of intercellular heterogeneity in various diseases. However, its full potentials for personalized medicine are yet to be reached. Towards this, we propose A Single-cell Guided pipeline to Aid Repurposing of Drugs (ASGARD). ASGARD can repurpose single drugs for each cell cluster and for multiple cell clusters at individual patient levels; it can also predict personalized drug combinations to address the intercellular heterogeneity within each patient. We tested ASGARD on three independent datasets, including advanced metastatic breast cancer, acute lymphoblastic leukemia, and coronavirus disease 2019 (COVID-19). On single-drug therapy, ASGARD shows significantly better average accuracy (AUC=0.95) compared to two other single-cell pipelines (AUC 0.69 and 0.57) and two other bulk-cell-based drug repurposing methods (AUC 0.80 and 0.75). The top-ranked drugs, such as fulvestrant and neratinib for breast cancer, tretinoin and vorinostat for leukemia, and chloroquine and enalapril for severe COVID19, are either approved by FDA or in clinical trials treating corresponding diseases. In conclusion, ASGARD is a promising pipeline guided by single-cell RNA-seq data, for repurposing personalized drugs and drug combinations. ASGARD is free for academic use at <https://github.com/lanagarmire/ASGARD>.

Introduction

Heterogeneity, or more specifically the diverse cell populations within the diseased tissue, is the main cause of treatment failure for many complex diseases, such as cancers ¹, Alzheimer's disease ², stroke ³, and coronavirus disease 2019 (COVID-19) ⁴, etc., as well as a major obstacle to successful personalized medicine ⁵⁻⁷. Recent significant advances of single-cell technologies, especially the single-cell RNA sequencing (scRNA-seq) technology, have enabled the analysis of intercellular heterogeneity at a very fine resolution ^{8,9} and helped us to have many breakthroughs in understanding the disease mechanisms¹⁰, such as breast cancer ¹¹, liver cancer ¹² and COVID-19 ¹³. However, its full potentials for personalized medicine have not been fulfilled ^{14,15}.

Drug repurposing (also known as drug reposition, reprofiling, or re-tasking) is a strategy to identify new uses of a drug outside the scope of its original medical approval or investigation ¹⁶. So far, very few drug repurposing methods have been developed to utilize the highly valuable information residing in scRNA-seq data. The pipeline by Alakwaa identifies significantly differentiated genes (DEGs) for a specific group of cells, then predicts candidate drugs for DEGs using the Connectivity Map Linked User Environment (CLUE) platform, followed by prioritizing these drugs using a comprehensive ranking score system ¹⁷. This pipeline identified didanosine as a potential treatment for COVID-19 using scRNA-seq data ¹⁷. Another pipeline by Guo et al. uses a simple combination of Seurat ¹⁸, a tool for scRNA-seq analysis, and CLUE to identify 281 FDA-approved drugs that have the potential to be effective for treating COVID-19 ¹⁹. However, the above pipelines predict drugs for each single-cell cluster within the patient but can't give comprehensive drug scores at the patient level. Meanwhile, in heterogeneous diseases caused by multiple types of cells, a combination of cell-targeting drugs has shown to be a better treatment strategy ²⁰. Neither of these above-mentioned pipelines is capable of predicting the combination of drugs, limiting their utility in the era of precision medicine.

Here we propose A Single-cell Guided pipeline for Accurate Repurposition of Drugs (ASGARD) to overcome the issue above. ASGARD repurposes single drugs for each population in single-cell data and predicts personalized drug combinations to address the intercellular heterogeneity within a patient. We applied ASGARD on several scRNA-seq datasets, including those from Patient-Derived Xenografts (PDXs) models of advanced metastatic breast cancers and from Pre-T acute lymphoblastic leukemia patients. The performance of ASGARD on single drugs is both more accurate and more robust compared to the two other pipelines mentioned earlier. Additionally, with the on-going worldwide COVID-19 pandemic, we applied ASGARD to scRNA-seq data from severe COVID-19 patients and predict potential therapies to reduce deaths of severe COVID-19 patients.

Methods

Single-cell RNA sequencing (scRNA-seq) data

We obtained scRNA-seq datasets from the Gene Expression Omnibus (GEO) database. Epithelial cells from Patient-Derived Xenografts (PDXs) models of 2 patients with advanced metastatic breast cancer and adult human breast epithelial cells from 3 healthy women are from GEO with accession numbers GSE123926 and GSE113197, respectively. ScRNA-seq data of pediatric bone marrow mononuclear cells (PBMMC) from 2 Pre-T acute lymphoblastic leukemia patients and 3 healthy controls are from GEO with accession number GSE132509. ScRNA-seq data of cells from bronchoalveolar lavage fluid (BALF) of 15 severe COVID-19 patients (4 deceased and 11 cured) are from GEO with accession numbers GSE145926 and GSE158055.

Processing of scRNA-seq data

ASGARD accepts processed scRNA-seq data from the Seurat package ¹⁸. In this study, genes identified in fewer than 3 cells are removed from the dataset. We used the same criteria as their original studies to filter cells ^{11,13,21}. Epithelial cells from breast cancer PDXs and healthy breast tissues with fewer than 200 unique genes are removed from the dataset. PBMC cells from leukemia patients and healthy controls with fewer than 200 unique genes are removed from the dataset. BALF cells from COVID-19 patients with fewer than 200 unique genes or more than 6000 unique genes or have a proportion of mitochondrial genes larger than 10% are removed from the dataset ¹³. We used cell cycle marker genes and linear transformation to scale the expression of each gene and remove the effects of the cell cycle on gene expressions.

Cell pairwise correspondences

ASGARD suggests using functions from Seurat for cell pairwise correspondences. In this study, gene counts for each cell were divided by the total counts for that cell and multiplied by a scaling factor (default is set to 10000). The count matrix was then transformed by $\log_2(\text{count}+1)$ in R. To identify gene variance across cells, we firstly fitted a line to the relationship of $\log(\text{variance})$ and $\log(\text{mean})$ using local polynomial regression (loess). Then we standardized the feature values using the observed mean and expected variance (given by the fitted line). Gene variance was then calculated on the standardized values. In this study, we used the 2,000 genes with the highest standardized variance for downstream analysis. Then we identified the K-nearest neighbors (KNNs) between disease and normal cells, based on the L2-normalized canonical correlation vectors (CCV). Finally, we built up the cell pairwise correspondences by identifying mutual nearest neighbors ¹⁸.

Cell clustering and annotation

We applied principal component analysis (PCA) from Seurat on the scaled data to perform the linear dimensional reduction. Then we used a graph-based clustering approach¹⁸. In this

approach, we firstly constructed a KNN graph based on the euclidean distance in PCA space and refined the edge weights between any two cell pairs using Jaccard similarity. Then we applied the Louvain algorithm of modularity optimization to iteratively group cell pairs together. We further ran non-linear dimensional reduction (UMAP) to place similar cells within the graph-based clusters determined above together in low-dimensional space. To annotate clusters of cells, we ran an automatic annotation of single cells based on similarity to the references single-cell panel using the SingleR package ²². We used the dominant cell type (>50% cells) as the cell type of the cluster.

Drug repurposing

ASGARD supports multiple methods for differential gene analysis, including Limma ²³, Seurat (Wilcoxon Rank Sum test) ¹⁸, DESeq2 ²⁴, and edgeR ²⁵. The differentially expressed gene list in a disease is transformed into a gene rank list. ASGARD uses 21,304 drugs/compounds with response gene expression profiles in 98 cell lines from the LINCS L1000 project ²⁶. A differential gene expression list in response to drug treatment is also transformed into a gene rank list. ASGARD further identifies potential candidate drugs that yield reversed gene expression patterns from that in the diseased vs. normal cells, using the DrInsight package ²⁷ (version: 0.1.1). Specifically, it identifies consistently differentially expressed genes, which are up-regulated in cells from diseased tissue but down-regulated in cells with drug treatment, or down-regulated in cells from diseased tissue but up-regulated in cells with drug treatment, to calculate the outlier-sum (OS) statistic ²⁸. The Kolmogorov–Smirnov test (K-S test) is then applied to the OS statistic, to show the significance level of one drug treatment relative to the background of all other drugs in the dataset. The reference drug dataset contains gene rank lists of 591,697 drug/compound treatments from the LINCS L1000 data, as mentioned above. The Benjamini-Hochberg (BH) false discovery rate (FDR) is used to adjust P-values from the K-S test to avoid false significance due to multiple hypothesis testing²⁹.

Drug score

ASGARD defines a novel drug score (Formula 1) to evaluate the treatment efficacy of single-drug and drug combinations on multiple single-cell clusters per sample. The drug score is a comprehensive estimation of drug therapeutic effects summing over every single cell cluster with weights. The drug score is estimated by the following formula:

$$Drug\ score = \sum_{k=1}^n \left(\frac{n.Cell_k}{Total.n.Cell} * (-\log_{10}^{FDR_k}) * \frac{Num(RevesedGene)_k}{Num(DiseasedGene)_k} \right) (1)$$

In this formula, k is a particular single-cell cluster. $Total.n.Cell$ is the total number of cells in the sample and $n.Cell_k$ is the number of cells in cluster k . FDR_k is the drug False Detective Rate (FDR) for cluster k . $Num(DiseasedGenes)_k$ is the number of significantly deregulated genes in cluster k , while $Num(ReversedGenes)_k$ is the number of significantly deregulated genes in cluster k that can be reversed by the drug. The ratio of reversed disease-related genes indicates the therapeutic effect of a drug for each cluster.

Besides the drug score, ASGARD further provides a Fisher's combined P-value³⁰ over the original P value of every cluster. It shows the drug significance on multiple single-cell clusters per sample. The combined p-value is calculated as the right-tail probability $P_{\chi^2(2n)}(T > t)$, where $t = -2 \sum_{i=1}^n \log_{10}^P_i$. The BH FDR is used to adjust Fisher's combined P-value.

For the drug combination, the user needs to set the number of drugs (size) in the combination. ASGARD explores all the potential combinations of required size, using significant drugs obtained from each cluster. It removes combinations that have adverse effects according to the data from Drugbank³¹ and SIDER database³². For the remaining combinations, ASGARD uses an additive model to estimate the combined gene expression response to the drug combination²⁰. The combined gene responses are then used to identify the reversely deregulated gene by the drug combination. If a gene is significantly up/down regulated in the diseased cluster k , and the gene

is reversely down/up regulated according to the combined gene response using additive model²⁰, then this gene is called the reversely deregulated gene by the drug combination. The drug combination score of combined drug A and drug B is modified from Formula 1, using Formula 2 below:

$$Drug\ combination\ score = \sum_{k=1}^n \left(\frac{n.Cell_k}{Total.n.Cell} * (-\log_{10}^{FDR_{ak}*FDR_{bk}}) * \frac{Num(RevesedGene)_{ck}}{Num(DiseasedGene)_k} \right) \quad (2)$$

In this formula, FDR_{ak} and FDR_{bk} are the FDRs of drug A and drug B for cluster k, respectively. $Num(RevesedGene)_{ck}$ is the number of the combined reversely deregulated genes by drug A and drug B in cluster k. Other terms have the same meanings as in Formula 1.

Performance comparison

We use the receiver operating characteristic curves (ROCs) and the areas under the ROC curves (AUCs) to compare the performance of ASGARD with those of the other two pipelines, as well as bulk methods. Since these pipelines/methods report both drugs and compounds, we let the ASGARD report both drugs and compounds in the comparisons with other pipelines/methods. For the performance estimation of ASGARD with different methods of differential gene analysis, we let the ASGARD only report drugs. ROCs and AUCs are calculated for each pipeline using the pROC package³³. True positive datasets in ROC and AUC estimation of single-drug are taken from FDA-approved drugs for the corresponding disease, as well as compounds and drugs in advanced clinical trials or have been proved effective in animal models. For the drug combination, the true positive dataset in ROC and AUC are taken from FDA-approved drug combinations or known synergistic drug-drug interactions on drug labels, from the Drugbank³¹ database. To assess the robustness of the three pipelines on different sizes of single-cell populations, simulation data are generated by randomly drawing the same number of disease and normal cells from GSE123926 and GSE113197 using the Bootstrapping method in R³⁴. To assess the robustness of the three pipelines on different similarities of single-cell populations, simulation data

are generated by adjusting differential gene expression levels from 20% to 90% of original differential levels of the single-cell cluster, based on GSE123926 and GSE113197. To assess the robustness of the three pipelines on unbalanced single-cell populations, simulation data are generated by randomly drawing 5000 cells with diseased cells proportion ranging from 20% to 90%. The true positive datasets, results of all the five methods, and scripts for the performance comparisons are available at: <https://github.com/lanagarmire/Single-cell-drug-repositioning/tree/master/ROC>

Code availability

ASGARD is available as an R package in Github (<https://github.com/lanagarmire/ASGARD>) under the PolyForm Noncommercial License.

Results

Summary of A Single-cell Guided pipeline to Aid Repurposing of Drugs (ASGARD)

Using scRNA-seq data, ASGARD repurposes drug combinations maximally efficiently for all cell populations, by fully accounting for the cellular heterogeneity of patients (Figure 1). In ASGARD, every cell type in the diseased sample is paired to that in the normal (or control) sample, according to “anchor” genes that are consistently expressed between diseased and normal cells. It then identifies consistently differentially expressed genes (P-value < 0.05) between the paired diseased and normal clusters in the scRNA-seq data, per computational methods including Limma²³, Seurat (Wilcoxon Rank Sum test)¹⁸, DESeq2²⁴ and edgeR²⁵. These individual clusters can be optionally annotated to specific cell types. Then ASGARD uses these consistently differentially expressed genes as inputs to identify drugs that can significantly (FDR < 0.05) reverse their expression levels in the L1000 drug response dataset, which comprises 591,697 drug/compound treatments²⁶. Specifically, ASGARD calculates the outlier-sum (OS) statistic first²⁸ by using the differentially expressed gene list, then applies the Kolmogorov–Smirnov test (K-S test) to the OS statistic to obtain the significance level of one drug treatment relative to the background of all other drugs in the reference drug dataset, as done before²⁷. Finally, ASGARD estimates the comprehensive drug score to identify single-drugs that are most efficient in treating all or selected diseased cell clusters (Formula 1 in Methods). ASGARD can also perform the drug combination analysis to identify the synergistic combination of repurposed drugs that are most potent in treating the selected diseased cell clusters (Formula 2 in Methods).

Comparing ASGARD to bulk-cell based repurposing methods

Before comparing ASGARD to other bulk RNA-Seq sample-based repurposing methods, we first determined the default differential expression method in ASGARD. For this, we compared several

representative differential expression methods: Limma ²³, Seurat (Wilcoxon Rank Sum test) ¹⁸, DESeq2 ²⁴, and edgeR ²⁵, using advanced metastatic breast cancer ^{11,21}, acute lymphoblastic leukemia³⁵, and coronavirus disease 2019 (COVID-19)^{13,36} datasets (see **Methods**). Drug prediction accuracies of ASGARD are determined by the receiver operating characteristic curves (ROCs) and the areas under the ROC curves (AUCs), using FDA-approved drugs and candidate drugs validated in advanced clinical trials as the true positive dataset. As shown in Figure 2A, limma yields the best AUCs for each of the three datasets with an average AUC 0.93 (0.90-0.98), significantly (P-value < 0.05, student's t-test) better than other differential expression methods. The AUCs for the other methods are: Seurat average 0.82 (0.80-0.86), DESeq2 average 0.83 (0.81-0.84), and edgeR average 0.87 (0.83-0.93). Therefore, limma was used as the default method in the ASGARD pipeline for the following analysis.

To compare ASGARD with those drug repurposing methods using bulk RNA-Seq samples, we summarized scRNA-seq data into pseudo-bulk RNA-Seq data. We then applied bulk methods CLUE ³⁷ and DrInsight ²⁷ on the pseudo-bulk RNA-Seq query data and compared their results with ASGARD on predicting both drugs and compounds (Figure 2B). We took the same scRNA-seq data from the same three datasets above. Since CLUE and DrInsight predict both drugs and compounds, we added compounds validated in animal models to the true positive dataset for the AUC evaluation of drug/compound predictions. As a result, the AUCs obtained from ASGARD on drugs and compounds (Figure 2B) are slightly different from those on drugs only (Figure 2A). On the breast cancer dataset, ASGARD yields an overall AUC of 0.92, much better than CLUE and DrInsight with values of 0.74 and 0.81 respectively. On precursor T-cell acute lymphoblastic leukemia data, ASGARD yields an AUC of 0.95 in drug/compound repurposing for the leukemia patients, while CLUE and DrInsight only achieve much worse averaged AUCs of 0.82 and 0.73 respectively. For the COVID-19 dataset, ASGARD shows an AUC of 0.97 in drug/compound repurposing for the deceased COVID-19 patients, while CLUE and DrInsight have much lower

AUCs of 0.85 and 0.72 respectively, on the same patients (Figure 2B). In summary, by paying attention to heterogeneity at single-cell levels, ASGARD shows much better drug repurposing predictability than methods that rely on bulk samples.

Comparing ASGARD to other single-cell based repurposing methods

We also compared single drug prediction using ASGARD with two other pipelines developed by Alakwaa et al.^{17,19} and Guo et al.^{17,19}, which were reported to handle scRNA-Seq data. Note that ASGARD offers more functionalities than those two methods, from at least two aspects. First, Alakwaa' and Guo' pipelines can only repurpose drug/compounds for each single-cell cluster but not on the patient level using multiple cell clusters. ASGARD on the other hand can compute both the cluster-level drug significance and the patient-level novel drug score (Formula 1 in **Methods**). Second, neither the Alakwaa' nor Guo' pipeline can propose drug combinations like ASGARD (Formula 2 in **Methods**). These unique functions of ASGARD will be demonstrated in the later sections. For a fair comparison, we tested single drug prediction accuracies of these three methods on individual clusters, which constitutes only a small portion of ASGARD's capacities (Figure 3, Supplementary Figure 1). ASGARD shows the best AUCs on every individual cluster from breast cancer, leukemia, and COVID-19 datasets (Figure 3). On the 8 clusters of breast cancer dataset, ASGARD yields an averaged AUC of 0.83 (0.80-0.86), much better (P-value<0.001, student's t-test) than Alakwaa' and Guo' pipelines, with averaged AUC values of 0.72 (0.62-0.79) and 0.56 (0.54-0.59) respectively (Figure 3A). On the 4 clusters of precursor T-cell acute lymphoblastic leukemia data, ASGARD has an averaged AUC of 0.81 (0.76-0.85), again much better (P-value<0.05, student's t-test) than Alakwaa' and Guo' pipelines, with averaged AUC values of 0.51 (0.49-0.56) and 0.52 (0.49-0.55) respectively (Figure 3B). Similar trends exist in the 4 clusters with increased cell proportions in the decreased severe vs cured severe COVID-19 patients (Figure 6A and 6B), with averaged AUCs of 0.87 (0.83-0.90), 0.81 (0.75-0.86), and 0.65 (0.61-0.68) for ASGARD, Alakwaa' and Guo' methods (Figure 3C). These

results collectively support the conclusion that ASGARD predicts single drugs more accurately than Alakwaa' and Guo' pipelines.

Additionally, given that sample size, cell population similarity, and proportion of disease cells impact significantly on differential gene analysis³⁸, we further performed robustness assessments of the three pipelines across different sizes of single-cell populations, different differential levels of single-cell populations, and different proportions of diseased cells using simulation data based on GSE123926 and GSE113197 dataset (see **Methods**). The AUCs of the three single-cell drug repurposing pipelines on the simulation data show that ASGARD, as well as the other two pipelines, have very robust performance across different sizes of single-cell populations (Supplementary Figure 2A), different degrees of differential expression between disease and normal conditions (Supplementary Figure 2B), and different proportions of disease cells among the scRNA-Seq data (Supplementary Figure 2C).

Single-cell drug repurposing for advanced metastatic breast cancer

We collected scRNA-seq data from 24,741 epithelial cells of advanced metastatic breast cancer Patient-Derived Xenografts (PDXs) models¹¹ and 16,998 epithelial cells from normal breast tissues²¹. After preprocessing, all cancer cells and 16,954 normal cells were paired and clustered into 8 populations (Figure 4A). Cluster 1 (C1) is the largest one covering 33.68% of cells, while cluster 8 (C8) is the smallest one accounting for only 1.8% of cells (Figure 4A). The differentially expressed genes (adjusted P-value <0.05, cancer vs normal) in the clusters are significantly enriched in 10 well-known breast cancer-related pathways, including including apoptosis, cell cycle, estrogen signaling, IL-17 signaling, neurotrophin signaling, NF-kappa B signaling, NOD-like receptor signaling, p53 signaling, PI3K-Akt signaling and TNF signaling pathways (Figure 4B). Cluster 7 (C7) has the largest number of 7 significant pathways, while C1 and C6 each have only 1 significant pathway.

We first applied ASGARD for single drug repurposing prediction and predicted 11 drugs (FDR<0.05 and overall drug score >0.99 quantiles) for advanced metastatic breast cancer (Figure 4C). Among them, fulvestrant and neratinib have been approved by the Food and Drug Administration (FDA) for breast cancer treatment^{39,40}. Fostamatinib is the top 1 drug candidate (Figure 4C). It is a tyrosine kinase inhibitor medication approved for the treatment of chronic immune thrombocytopenia⁴¹. We next applied ASGARD to predict drug combinations, using significant drugs (FDR<0.05) repurposed for each cluster (Table 1, Supplementary Table 1). We used drug combinations approved for breast cancer or having known synergistic drug-drug interactions as the true positive dataset in the AUC estimation. ASGARD shows an AUC of 0.85 in predicting drug combinations for advanced metastatic breast cancer (Figure 4D). Fostamatinib and colchicine are proposed as the top 1 drug combination (Figure 4E). Colchicine is an alkaloid approved for treating the inflammatory symptoms of familial Mediterranean fever⁴².

We next investigated the target genes and pathways of fostamatinib and colchicine combination (Figure 4F). Fostamatinib and colchicine both target all the significant pathways in each cluster. Fostamatinib and colchicine are complementary in targeting genes of these pathways. Among the 143 target genes from these significant pathways, only 29 target genes are shared by fostamatinib and colchicine (Figure 4F). The combination of fostamatinib and colchicine also shows biologically synergistic targeting of multiple genes on the same significant pathways. For example, fostamatinib inhibits Cyclin D1 (CCND1) to produce G1 arrest in the p53 signaling pathway, while colchicine inhibits Cyclin-dependent kinase 1 (CDK1) to produce G2 arrest in the p53 signaling pathway and cell cycle pathway⁴³ (Figure 4F). Additionally, the drug scores of top drug combination candidates vary from one PDX model to another (Figure 4E), demonstrating that ASGARD is a forward-looking personalized medicine strategy *in silico*.

Single-cell drug repurposing for precursor T-cell acute lymphoblastic leukemia (Pre-T ALL)

We further applied ASGARD to the collected scRNA-seq data from 2 Pre-T ALL patients and 3 normal healthy controls³⁵. ASGARD identifies 8 types of cells (Figure 5A), in which T cells are further clustered into 4 sub-populations (Figure 5B). Cluster 1 (C1) is the largest one covering 47.29% of cells, while cluster 4 (C4) is the smallest accounting for only 2.11% of cells (Figure 5B). The differentially expressed genes (adjusted P-value <0.05, Pre-T ALL vs normal) in the T cell clusters are significantly enriched in 6 pathways, including apoptosis, cell cycle, cGMP–PKG signaling, NF–kappa B signaling, p53 signaling, and T cell receptor signaling pathways (Figure 5C). Among the predicted drugs by ASGARD, the 1st candidate tretinoin and 6th candidate vorinostat have been approved for the treatment of leukemia^{44,45} (Figure 5D, Supplementary Table 2). Tretinoin is a vitamin A derivative. Tretinoin targets many genes in all 4 clusters, such as MDM4, a regulator of p53 (MDM4) in the p53 signaling pathway, cyclin D3 (CCND3) in cell cycle and p53 signaling pathways, G protein subunit alpha q (GNAQ) and phospholipase C beta 1 (PLCB1) in the cGMP–PKG signaling pathway, Fos proto-oncogene (FOS) and p21 (RAC1) activated kinase 2 (PAK2) in T cell receptor signaling pathway, spectrin alpha non-erythrocytic 1 (SPTAN1) in apoptosis pathway and zeta chain of T cell receptor associated protein kinase 70 (ZAP70) in apoptosis and NF–kappa B signaling pathways (Figure 5E). All these genes were previously shown significance in T cell clusters of ALL^{46–48}.

Single-cell drug repurposing for severe patients with coronavirus disease 2019 (COVID-19)

Using ASGARD, we annotated scRNA-seq data collected from the bronchoalveolar lavage fluid (BALF) of 15 severe COVID-19 patients^{13,36}. ASGARD identified 7 types of cells, including 6 types of immune cells and epithelial cell types (Figure 6A). Monocyte is the largest cell population in both deceased and cured severe COVID-19 patients (Figure 6B). The population of neutrophil, NK cell, T cell, and monocyte increased in deceased severe COVID patients compared to the cured ones, suggesting the important role of these four types of cells in the COVID19-related

death⁴⁹⁻⁵² (Figure 6B). The differentially expressed genes (adjusted P-value <0.05, deceased severe vs cured severe) in the four types of cells are significantly enriched (adjusted P-value <0.05) in 8 pathways, including chemokine signaling, coronavirus disease-COVID-19, IL-17 signaling, JAK-STAT signaling, NF-kappa B signaling, T cell receptor signaling, TNF signaling and Toll-like receptor signaling pathways (Figure 6C). Coronavirus disease-COVID-19 pathway is the most significant pathway in these cells. Chemokine signaling, NF-kappa B signaling, TNF signaling, and Toll-like receptor signaling pathways are the most widely enriched pathways in all four types of cells. T cell receptor signaling pathway is only enriched in T cells.

We thus applied ASGARD to identify single drug candidates that target the four cell types, including neutrophil, NK cell, T cell, and monocyte, in the hope to reduce the mortality of severe COVID-19. Among the drugs predicted to reduce the mortality of the severe COVID-19 patients, rescinnamine (2nd) and enalapril (4th) caught our attention (Figure 6D, Supplementary Table 3). Both rescinnamine and enalapril are angiotensin-converting enzyme (ACE) inhibitors. Rescinnamine and enalapril share most of the key genes on all the significant pathways in monocyte, NK cell, neutrophil, and T cell, respectively (Figure 6E). In monocyte, rescinnamine and enalapril share 47 key target genes, including Janus Kinase 1 (JAK1), Janus Kinase 2 (JAK2), C-C Motif Chemokine Ligand 2 (CCL2), C-C Motif Chemokine Ligand 4 (CCL4), and C-C Motif Chemokine Ligand 8 (CCL8), and all the 7 significant pathways. In NK cells, rescinnamine and enalapril share 35 key target genes from 6 significant pathways, such as JAK1, Janus Kinase 3 (JAK3), CCL4, tumor necrosis factor (TNF), and Signal Transducer And Activator Of Transcription 2 (STAT2). In neutrophils, rescinnamine and enalapril share 16 key target genes, such as CCL2, CCL8, C-X-C Motif Chemokine Ligand 8 (CXCL8) and C-X-C Motif Chemokine Ligand 10 (CXCL10), and all the 5 significant pathways. In T cell, rescinnamine and enalapril share 30 key target genes, such as CCL2, CCL8, C-X-C Motif Chemokine Ligand 9 (CXCL9), JAK3, TNF, and Lymphocyte Cytosolic Protein 2 (LCP2), and all the 6 significant pathways of T cell. The shared

target genes and pathways in corresponding cells were previously shown related to death from COVID19⁴⁹⁻⁵².

Discussion

In this study, we present A Single-cell Guided pipeline to Aid Repurposing of Drugs (ASGARD). To evaluate the accuracy of ASGARD in single drug repurposing, we compared ASGARD to other repurposing methods that utilize bulk cell RNA-Seq (CLUE and DrInsight) or single-cell RNA-Seq data (Alakwaa's and Guo's) on a variety of diseases, including breast cancer, leukemia, and COVID-19. ASGARD shows much better performance than all of these methods in predicting drug/compounds (Figure 2, 3, Supplementary Figure 1). The performance of ASGARD is also robust across different sizes and proportions of cell populations, as well as differential expression levels (Supplementary Figure 2). Moreover, we highlight that ASGARD can not only summarize drug efficiency across all clusters at the individual patient level but also propose drug combinations. These important functions are missing in other simple single-cell RNA-Seq drug reposition pipelines of Alakwaa and Guo.

ASGARD achieves overall drug ranking for the disease/patient, by a novel drug score that evaluates the treatment efficacy across all/selected single-cell clusters (Formula 1 in **Methods**). This drug score shows a significantly (P -value <0.05 , student's t -test) better AUC than the prediction based on individual clusters (Figure 2, 3). It suggests that targeting individual cell clusters isn't sufficient for treating diseases. Good therapy should be able to target all essential diseased cell clusters of the patient. On the other hand, it is not ideal to propose drug repurposing using bulk RNA-seq as done by traditional methods either (eg. CLUE and DrInsight). There exists significant heterogeneity of different cell populations and not all these cells play equal roles in the

diseases^{53,54}, reflected by different gene expression responses to drug treatment⁵⁵. ASGARD can distinguish more important cell types from others and repurpose drugs accordingly, explaining why ASGARD has significantly (P-value <0.05, student's t-test) better AUC performance than traditional bulk methods (Figure 2B). Moreover, ASGARD also demonstrates variations of drug and drug combination scores within patients (Figure 4C, 4E, 5D, and 6D). This stresses that personalized therapy is necessary for the best therapeutic effect and utilizing single-cell sequencing information may help to achieve that.

We chose breast cancer or leukemia datasets to illustrate the utilities of ASGARD, given the relative abundance of prior knowledge on drugs. Many drugs predicted by ASGARD have been approved by FDA, such as fulvestrant and neratinib for breast cancer^{39,40} (Figure 4C), tretinoin, and vorinostat for leukemia^{44,45} (Figure 5D). The drug combination is an alternative strategy to precisely addressing multiple diseased single-cell clusters. In the breast cancer dataset, fostamatinib and colchicine is the top 1 candidate combination (Figure 4E). Fostamatinib is a tyrosine kinase inhibitor. Tyrosine kinase inhibitors have been widely used either in single drug treatment or combination therapy for breast cancer^{56,57}. Colchicine is an alkaloid used in symptomatic pain relief in attacks of gout. Fostamatinib and colchicine show synergistic targeting of multiple genes in the significant pathways associated with breast cancers (Figure 4F). For example, fostamatinib inhibits Cyclin D1 (CCND1) to produce G1 (first growth) arrest⁵⁸ in the p53 signaling pathway, and colchicine inhibits Cyclin-dependent kinase 1 (CDK1) to produce G2 (second growth) arrest⁵⁹ in the p53 signaling pathway and cell cycle pathway. G1 and G2 are important phases of the cell cycle, essential for the treatment of breast cancer⁶⁰. The combination of colchicine and fostamatinib shows a synergistic effect according to the drug interaction record from the DrugBank database³¹, although it hasn't been tested in breast cancer in particular.

COVID-19 is an ongoing and evolving pandemic, therefore drug knowledge is changing too. Remdesivir is the only drug approved for COVID-19⁶¹. But it's not in the L1000 drug response

dataset, and therefore wasn't predicted by ASGARD. However, ASGARD does predict ACE inhibitors rescinamine and enalapril as the 2nd and 4th drug candidates, aimed to reduce the mortality of the severe COVID-19. A study of 19,486 COVID-19 patients from 8.28 million England participants showed that enalapril was associated with reduced risks of COVID-19 disease⁶². Another observational clinical trial on 22,213 participants (ClinicalTrials.gov Identifier: NCT04467931) further showed that the use of enalapril is associated with a 15% lower relative risk of mortality of COVID-19 patients⁶³. Our drug-gene-pathway analysis shows that enalapril targets all the significantly deregulated pathways, such as coronavirus disease–COVID–19, chemokine signaling, and IL–17 signaling pathway, in monocyte, NK cell, neutrophil, and T cell (Figure 6E). These pathways play important roles in COVID-19 patient severity and survival⁶⁴. It may explain the observed efficiency of enalapril in reducing mortality of COVID-19 patients. On the other hand, rescinamine was rarely studied for COVID-10. Since rescinamine targets the same significant pathways as enalapril in COVID-19 (Figure 6E), rescinamine could be an alternative candidate for further investigation.

Altogether, this study shows clear evidence that ASGARD repurposes confident drugs that were approved or in clinical trials for breast cancer, leukemia, and COVID-19, respectively. It also provides new applications for drugs and drug combinations that warrant further clinical studies. In all, ASGARD is a single-cell guided pipeline with significant potential to recommend personalized repurposeful drugs and drug combinations using scRNA-seq data.

Acknowledgments

The authors thank Qianhui Huang, Yuheng Du and Mohammad Vahed for helping with the manuscript, Duxin Sun, Joseph Burnett and Jamie Do for the helpful discussions, Yijun Li for testing the ASGARD package.

Funding

This research was supported by the National Institute of Environmental Health Sciences through funds provided by the trans-NIH Big Data to Knowledge (BD2K) initiative [K01ES025434]; the US National Library of Medicine [R01 LM012373, R01 LM12907]; and the National Institute of Child Health and Human Development [R01 HD084633; to L.X. Garmire].

Author contributions

L.X. Garmire conceived the study of and supervised the project. B. He wrote the code and analyzed the data. B. He and L.X. Garmire wrote the manuscript.

Competing interests

The authors declare that they have no competing interests.

Data and materials availability

ScRNA-Seq data are available in Gene Expression Omnibus (Accession number: GSE123926, GSE113197, GSE132509, GSE158055, and GSE145926). Phase I LINCS L1000 data are available in Gene Expression Omnibus (Accession number: GSE92742). Phase II LINCS L1000 data are available in Gene Expression Omnibus (Accession number GSE70138). ASGARD is available as an R package in Github (<https://github.com/lanagarmire/ASGARD>). Scripts used in this study are available in Github (<https://github.com/lanagarmire/Single-cell-drug-repositioning>).

Table 1. Single-cell clusters and candidate drugs for the advanced metastatic breast cancer PDX model.

Cluster	Proportion(%)	Drug		Key genes
		Drug name*	FDR	
C1	33.68	fostamatinib	6.48E-03	SFN, GADD45A, CDKN1A, CYCS, IGFBP3, CDKN2A, EI24, SIVA1, PMAIP1, BAX, TP53I3, AIFM2, TNFRSF10A, GADD45B
		fulvestrant	3.17E-03	
C2	23.33	fostamatinib	1.44E-03	RHOA, CXCL8, VDAC1, TXN, BIRC3, CASP4, CYBA, IFI16, CXCL1, VDAC2, ATG12, TXNIP, NFKBIA, GBP2, HSP90AA1, CXCL2, TRAF2, YWHAE, MAPK8, JAK1, RELA, NAMPT, FOSL1, HSP90B1, FOS, FOSB, S100A9, CALML5, ARHGDI, ATF4, RAP1B, HRAS, IRS1, CDC42, CALML3, IRAK2, GRB2, CAPN2, TNFRSF10A, CTSC, TUBA1C, EIF2S1, ACTG1, PMAIP1, GADD45B, GADD45A, TUBA4A, TUBA1B, CASP7
		colchicine	2.11E-03	
		sirolimus	5.83E-04	
C3	13.03	vincristine	1.75E-01	CAPN2, TUBA1B, TUBA1C, EIF2S1, FOS, ACTG1, PMAIP1, ATF4, GADD45B, GADD45A, JUN, BAX, BIRC3, AKT2, BBC3, NFKBIA, TNFRSF10A, CTSC
C4	11.15	fulvestrant	4.41E-02	KRT18, FOS, KRT19, KRT17, KRT23, CALML5, HSPA8, CALM3, KRT14, GNAQ, CALM2, HSP90AA1, GNAI2, PIK3R3, SHC1, JUN, CALML3, PIK3R1, CREB3L4, HSP90B1, CREB5, KRT15, NR4A1, YWHAH, RPS6, COL9A2, YWHAZ, COL1A2, NGF, RAC1, LAMB3, ITGA3, MYC, ITGB4, ITGA2, PPP2R5A, FOXO3, ITGB6, PRLR, SGK1, COL6A2, DDIT4, COL9A3, GNG5, PTK2, COL2A1, OSMR, FGFR1, PDGFC, RHEB, ARHGDI, RIPK2, MAPK13, BAX, SFN, CDKN2A, HDAC2, CDKN2C, RAD21, TFDP1, CDK1, WEE1, MCM3, PCNA, CDC20, MAD2L2, E2F3, SMC1B, SKP1, ANAPC16, MCM6, PKMYT1
		crizotinib	7.76E-04	
		neratinib	1.52E-02	
		pazopanib	3.78E-02	
C5	8.51	fostamatinib	2.63E-07	SFN, PMAIP1, IGFBP3, CDKN2A, GADD45B, GADD45A, CCND2, BBC3, AIFM2, CDKN1A, SERPINE1, EI24, TNFRSF10A, BAX, BIRC3, CXCL1, SOCS3, ATF4, ICAM1, AKT3, MAP2K3, CASP7, CCL2, JAG1, FOS, IL15, TRAF1, NFKBIA, MMP14, CXCL6, CXCL8, IFI16, CASP4, GBP2, RHOA, IRF7, TXNIP, VDAC1, VDAC2, CASP1, GBP3, JAK1, ATG12, NAMPT, CYBA, TXN, CARD16, ACTG1, CTSC, TUBA1C, HRAS, CAPN2, EIF2S1, TUBA1B
C6	5.43	fostamatinib	5.05E-03	SFN, CDKN2A, CYCS, IGFBP3, EI24, CCND1, PERP, CCND2, CD82, GADD45A, SERPINE1, DDB2, CDK1, TP53I3, SERPINB5
		mebendazole	7.37E-04	
C7	3.08	fostamatinib	1.12E-06	CXCL2, CXCL1, ICAM1, AKT3, TNFAIP3, CCL2, RIPK3, CXCL6, SOCS3, FAS, MAP2K3, ATF4, NFKBIA, TRAF1, CASP7, PIK3CD, IL15, CSF1, JUN, BIRC3, GBP2, CXCL8, IFI16, IRF7, CARD18, CASP4, CARD16, RHOA, VDAC1, CTSB, CASP1, TICAM1, MAP1LC3B, HSP90AA1, GBP1, YWHAE, ATG12, S100A9, FOSL1, S100A8, IL17B, TRAF3IP2, TRAF4, HSP90B1, SFN, PMAIP1, GADD45B, CCND2, CDKN2A, BBC3, CYCS, TP53AIP1, GADD45A, IGFBP3, PERP, SERPINE1, PLAU, NFKB2, CD40, RELB, BCL10, CALML3, CALML5, IRS1, ARHGDI, IRAK2, ARHGDI, CAMK2B, NGFR, GRB2, ACTG1, CTSC, TNFSF10, TUBA1A, CAPN2, TUBA1C, CTSC
C8	1.8	colchicine	3.49E-05	FOS, BIRC5, CTSF, CASP2, ITPR2, LMNB1, ATF4, ENDOG, PARP1, HRK, TUBA1C, CAPN2, GADD45B, EIF2S1, ACTG1, CDKN2A, MAD2L1, CCNA2, CCNB2, CCNB1, SKP1, E2F5, PRKDC, SKP2, ORC6, ORC1, TTK, PTTG1, YWHAH, CDKN2C, SFN, MCM6, CCNE2, CCNE1, RBL1, CDC20
		mebendazole	3.49E-05	

*: The best candidate drug and significant drugs with $FDR < 0.05$ for each cluster are shown in this table.

Figure Legends

Figure 1. The workflow of the ASGARD drug repurposing pipeline. The workflow of the ASGARD pipeline. Diseased and normal cells are paired according to “anchor” genes that are expressed consistently between the two types of cells. The differentially expressed (DE) genes are identified between diseased and normal cells, either within a cluster or within a cell type. Using the consistently DE genes as the input, potential drugs that significantly reverse the pattern of DE genes are identified, using the Kolmogorov–Smirnov (K-S) test with Benjamini-Hochberg (BH) false discovery rate (FDR) adjustment. Next ASGARD estimates and ranks the comprehensive drug scores for single drugs or the drug combination scores for drug combinations, by targeting specific cell cluster(s) or all cell clusters.

Figure 2. Comparing ASGARD to bulk-cell-based repurposing methods. (A) The receiver operating characteristic (ROC) curves and area under curve (AUC) scores of the ASGARD, using DE analysis methods (Limma, DESeq2, Seurat, and edgeR). The tests are done on advanced metastatic breast cancer, acute lymphoblastic leukemia, and coronavirus disease 2019 (COVID-19), respectively. DESeq2 failed to produce results over 82,157 cells in COVID-19 data. **(B)** ROC curves and AUC scores of the ASGARD and bulk-cell based drug repurposing methods (CLUE and DrInsight), using the same three diseases as in **(A)**. The single-cell RNA-Seq data were aggregated to pseudo-bulk RNA-Seq data for the bulk-cell-based methods.

Figure 3. Comparing ASGARD to other single-cell-based repurposing methods. ROC curves and AUC scores of the ASGARD and other published pipelines (Alakwaa’s pipeline and Guo’s pipeline). The results of drug/compound repurposing are shown on every cell cluster of the metastatic breast cancer dataset **(A)**, every cell cluster of acute lymphoblastic leukemia dataset **(B)** and 4 clusters with increased cell proportions in the decreased severe vs cured

severe COVID-19 patients **(C)**. The proportion of each single-cell cluster is shown in the brackets above each plot.

Figure 4. Drug repurposing in Patient-Derived Xenograft (PDX) models from advanced metastatic breast cancers. **(A)** UMAP plots of single-cell data from 3 normal controls and 2 breast cancer PDX samples. **(B)** Pathway enrichment analysis (breast cancer vs normal) for each single-cell cluster. **(C)** The overall drug score combining both PDX models and drug score in each breast cancer PDX model, among top-ranked significant single drugs (FDR<0.05). Drugs approved for breast cancer treatment by the FDA are labeled in red boxes. **(D)** ROC curve and AUC scores of the ASGARD in the drug combination prediction for breast cancer. **(E)** The overall drug score combining both PDX models and drug score in each breast cancer PDX model, among top-ranked significant drug combinations (FDR<0.05). **(F)** The drug candidates fostamatinib and colchicine, their target genes, pathways, and single-cell clusters. Orange node: up-regulated gene ($\log_{2}FC > 1$ and adjusted P-value < 0.05). Blue node: down-regulated gene ($\log_{2}FC < -1$ and adjusted P-value < 0.05). Orange solid edge: drug stimulates gene expression. Blue solid edge: drug inhibits gene expression. The width of the edge is proportional to the strength of the drug effect. Grey dotted edge: gene belonging to a pathway. Grey backward slash: pathway significant in a cell cluster.

Figure 5. Drug repurposing for precursor T-cell acute lymphoblastic leukemia (Pre-T ALL). **(A)** UMAP plots of all cells from 3 normal controls and 2 Pre-T ALL samples. **(B)** UMAP plots of T cell clusters from normal controls and Pre-T ALL samples. **(C)** Pathway enrichment analysis (leukemia vs normal) for each T cell cluster. **(D)** The overall drug score and drug score in each Pre-T ALL patient, among top-ranked significant drugs (FDR<0.05). **(E)** The drug candidate tretinoin, its target genes, pathways, and single-cell clusters. All labels and their annotations are the same as Figure 4F.

Figure 6. Drug repurposing for reducing mortality of severe COVID-19 patients. (A) Single-cell populations of bronchoalveolar immune cells in 11 cured and 4 deceased severe COVID-19 patients, respectively. **(B)** The proportions of cell type in (left) and log10 transformed fold changes in deceased over the cured state (right) of the single-cell populations in (A). **(C)** Pathway enrichment analysis (deceased severe vs cured severe) for neutrophil, NK cell, T cell, and monocyte respectively. **(D)** The drug scores in each of the four deceased severe COVID-19 patients as well as all four patients, among top-ranked significant drugs (FDR<0.05). **(E)** The drug candidate rescinnamine and enalapril, their target genes and pathways in the monocyte, NK cell, T cell, and neutrophil, respectively, from severe COVID-19 patients. All labels and their annotations are the same as Figure 4F.

Supplementary Materials

Supplementary Figure 1. Boxplots on AUCs of the three single-cell-based repurposing pipelines, based on all cell clusters as shown in Figure 3.

Supplementary Figure 2. AUC scores of the three single-cell-based repurposing pipelines, using simulation data adapted from the real datasets. (A) The effect of varying total cell sizes from 100 cells to 20000 cells. **(B)** The effect of varying differential expression levels from 20% to 90%. **(C)** The effect of varying the proportions of diseased cells ranging from 20% to 90%.

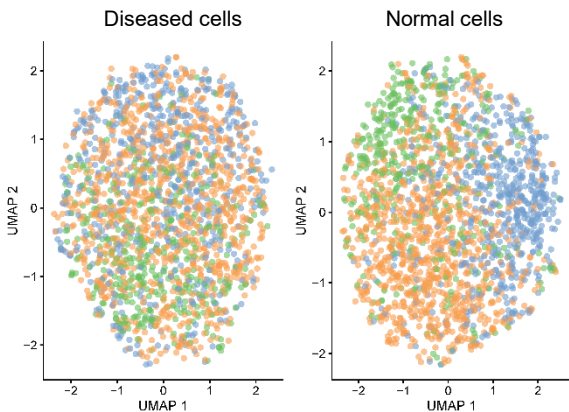
Supplementary Table 1. Individual drug significances and overall drug scores for breast cancer.

Supplementary Table 2. Individual drug significances and overall drug scores for leukemia.

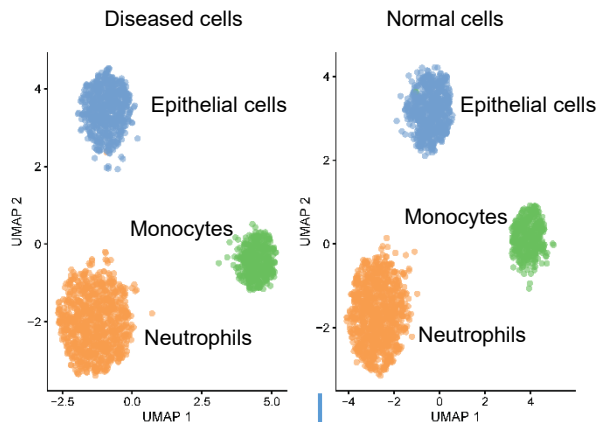
Supplementary Table 3. Individual drug significances and overall drug scores for COVID-19.

Figure 1

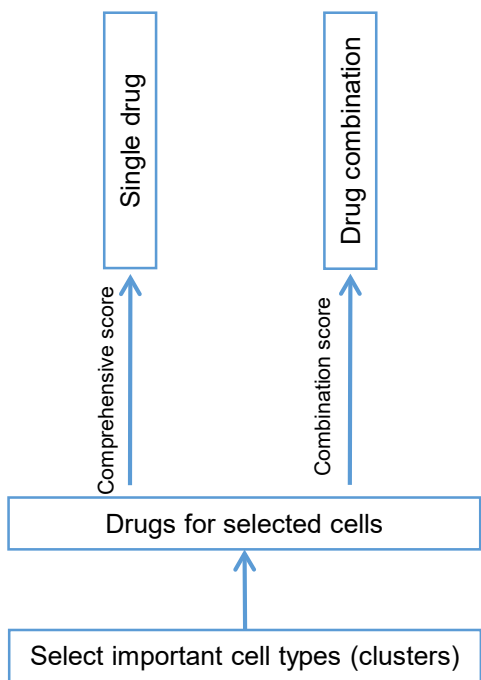
Cell pairwise correspondence



Cell clustering and annotation



Drug selection



Drug reposition

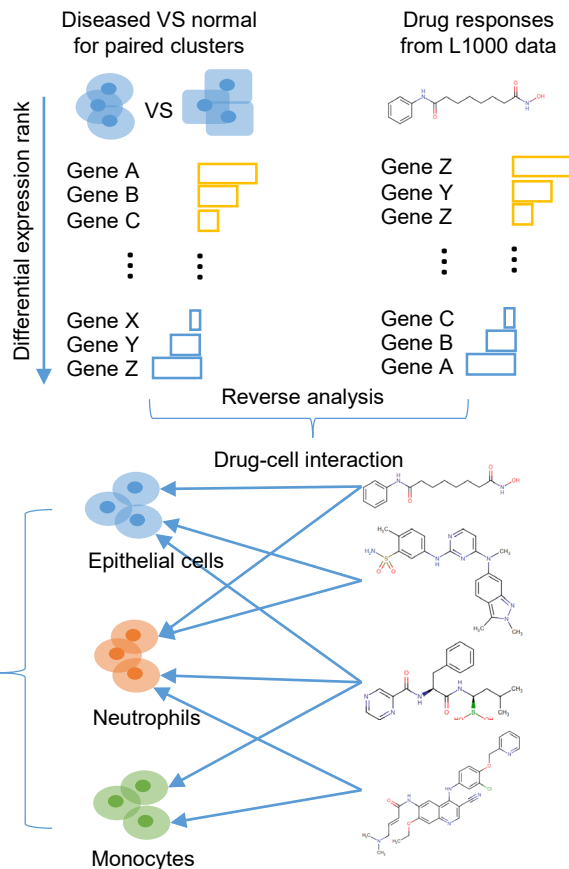


Figure 2

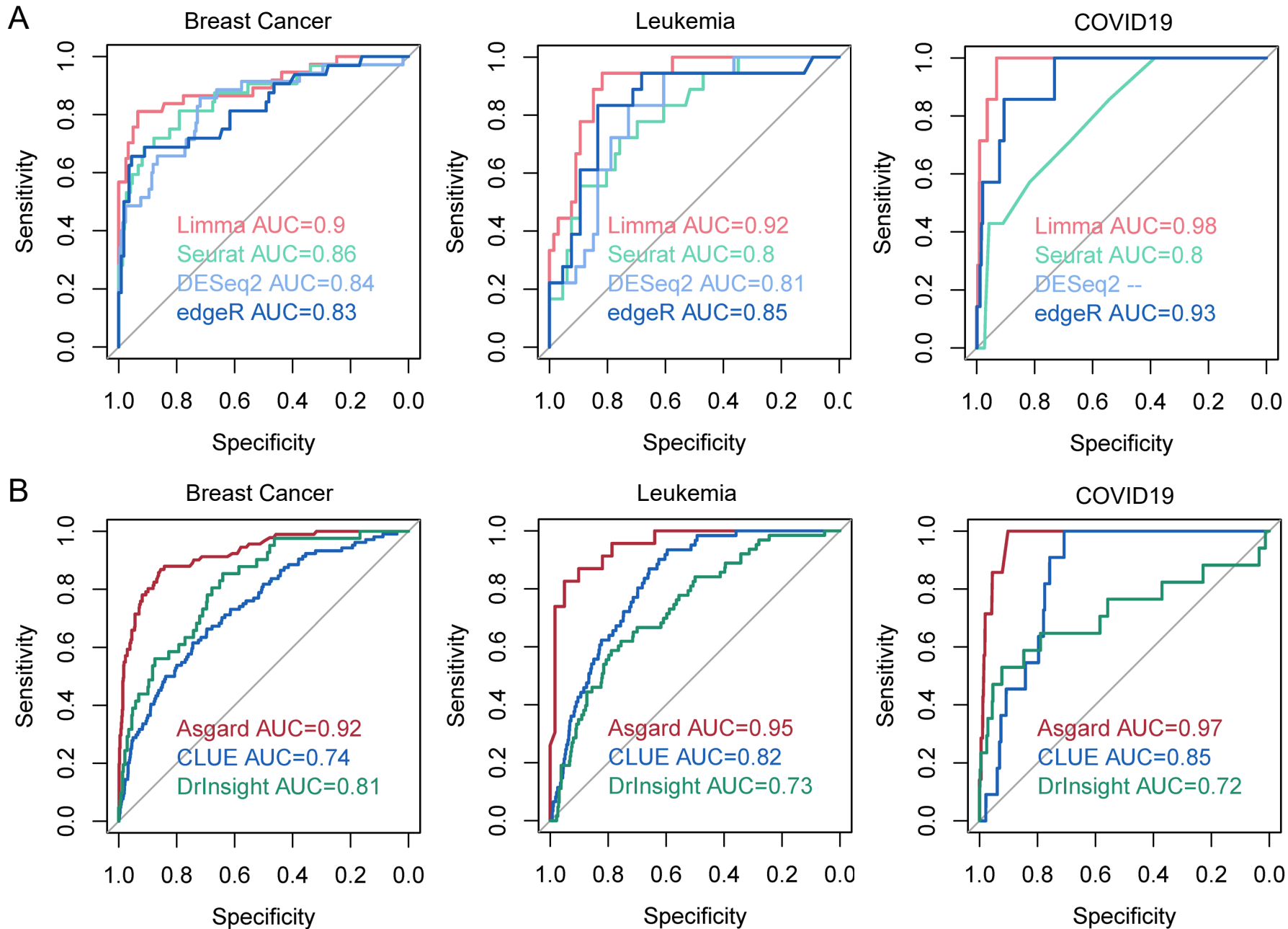
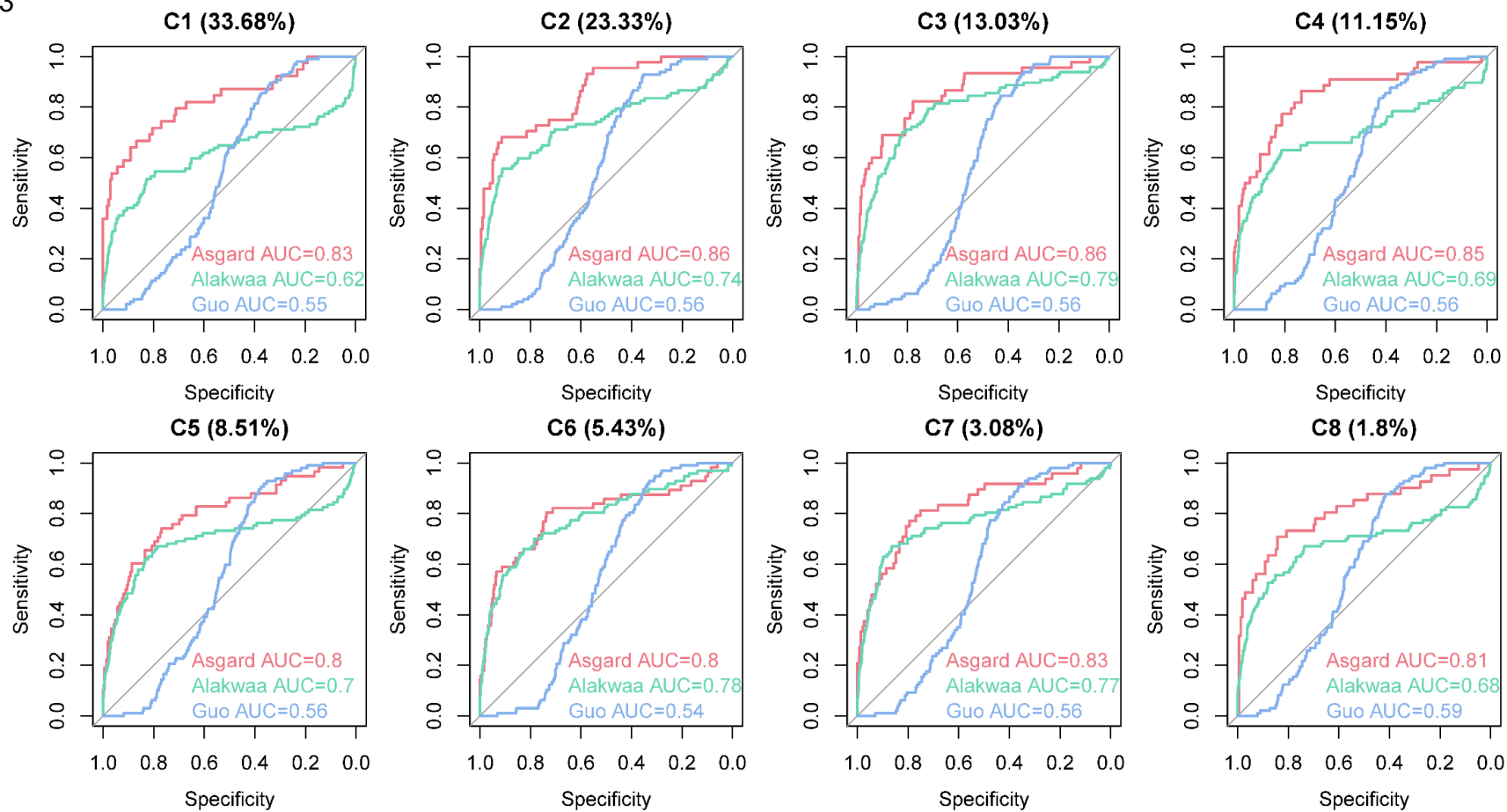


Figure 3

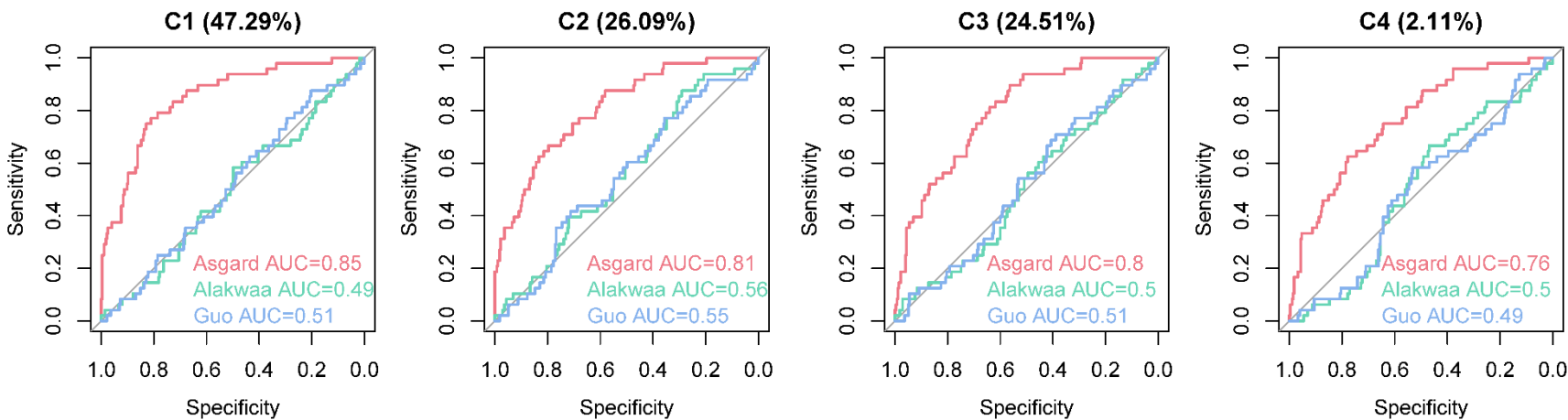
A

Breast Cancer



B

Leukemia



C

COVID19

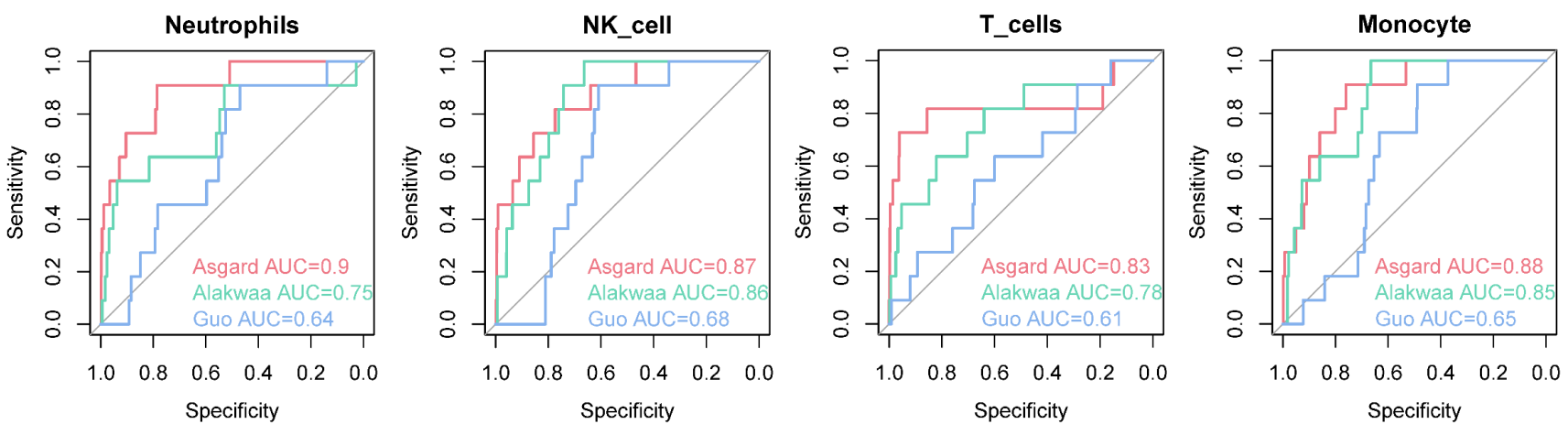
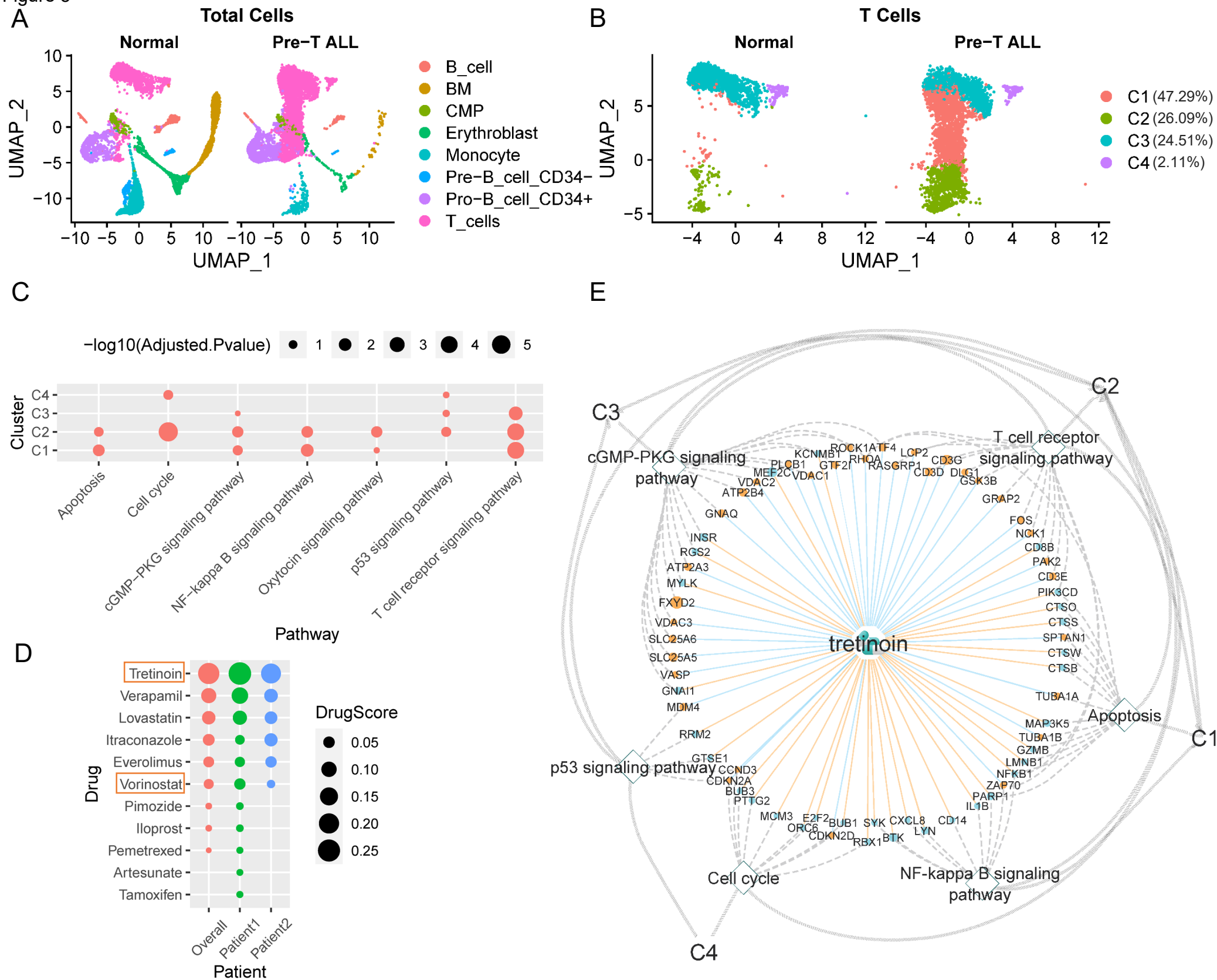
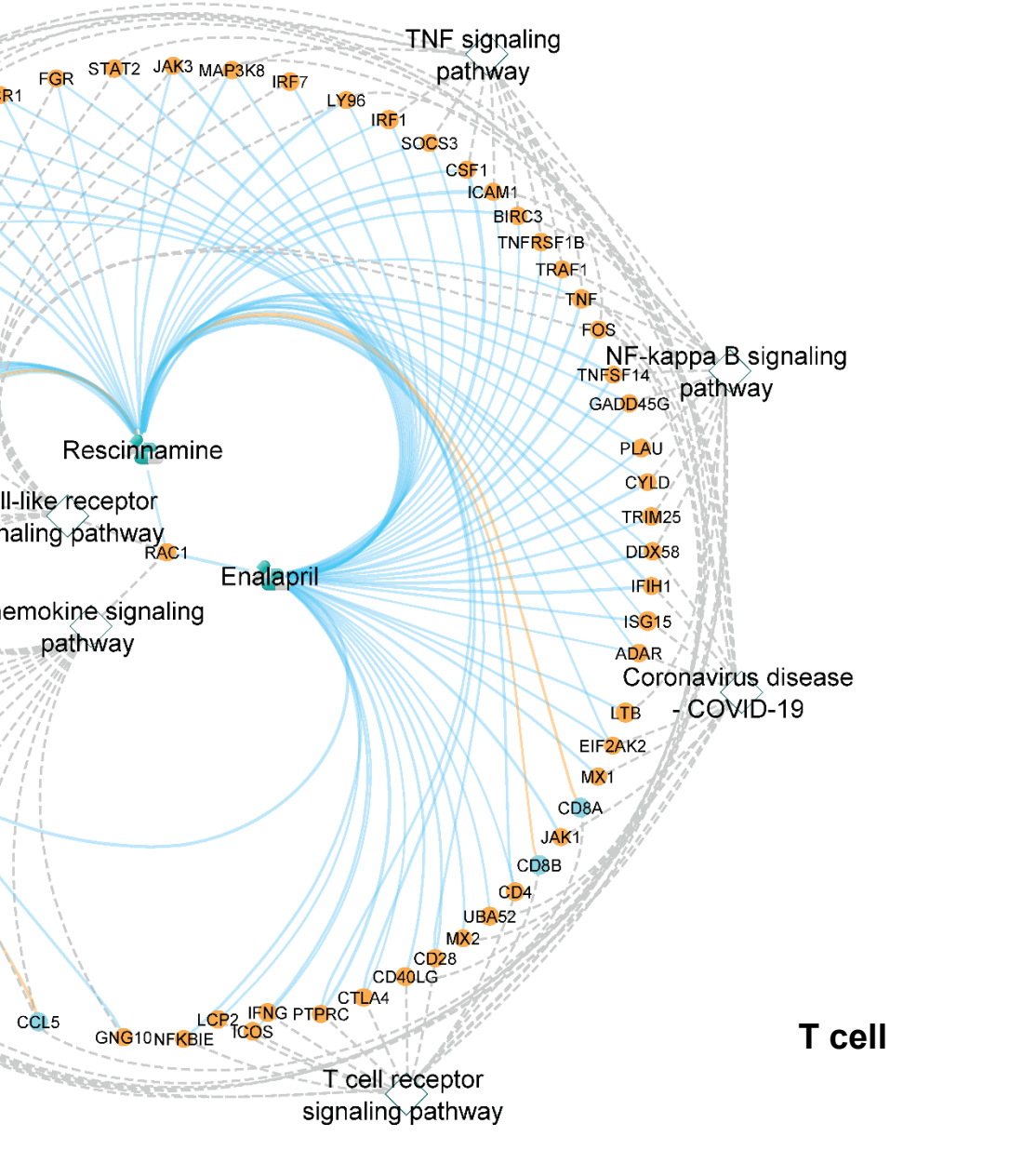
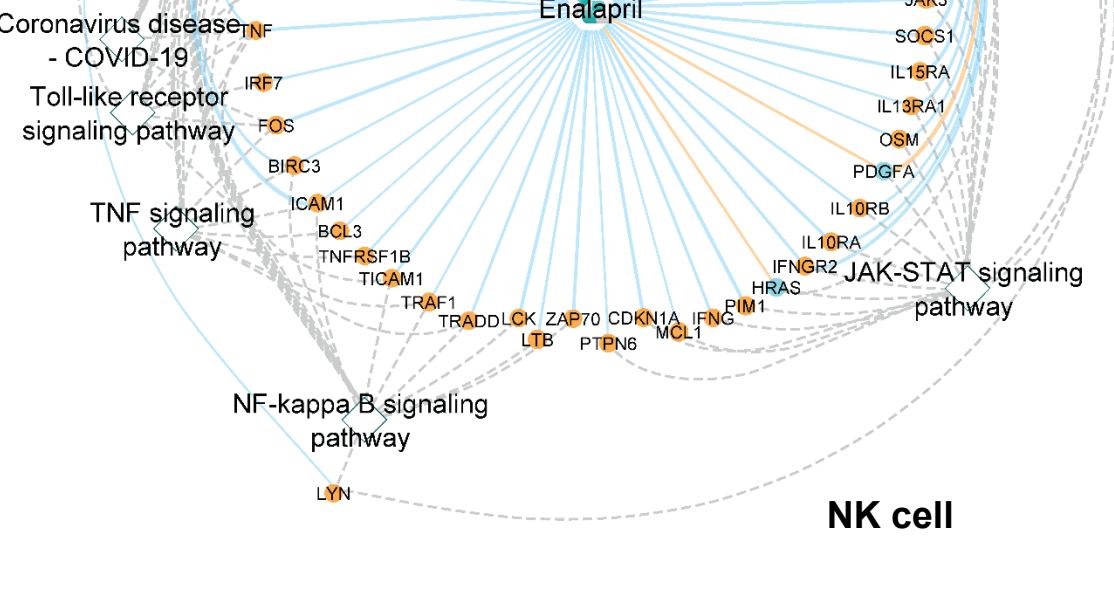
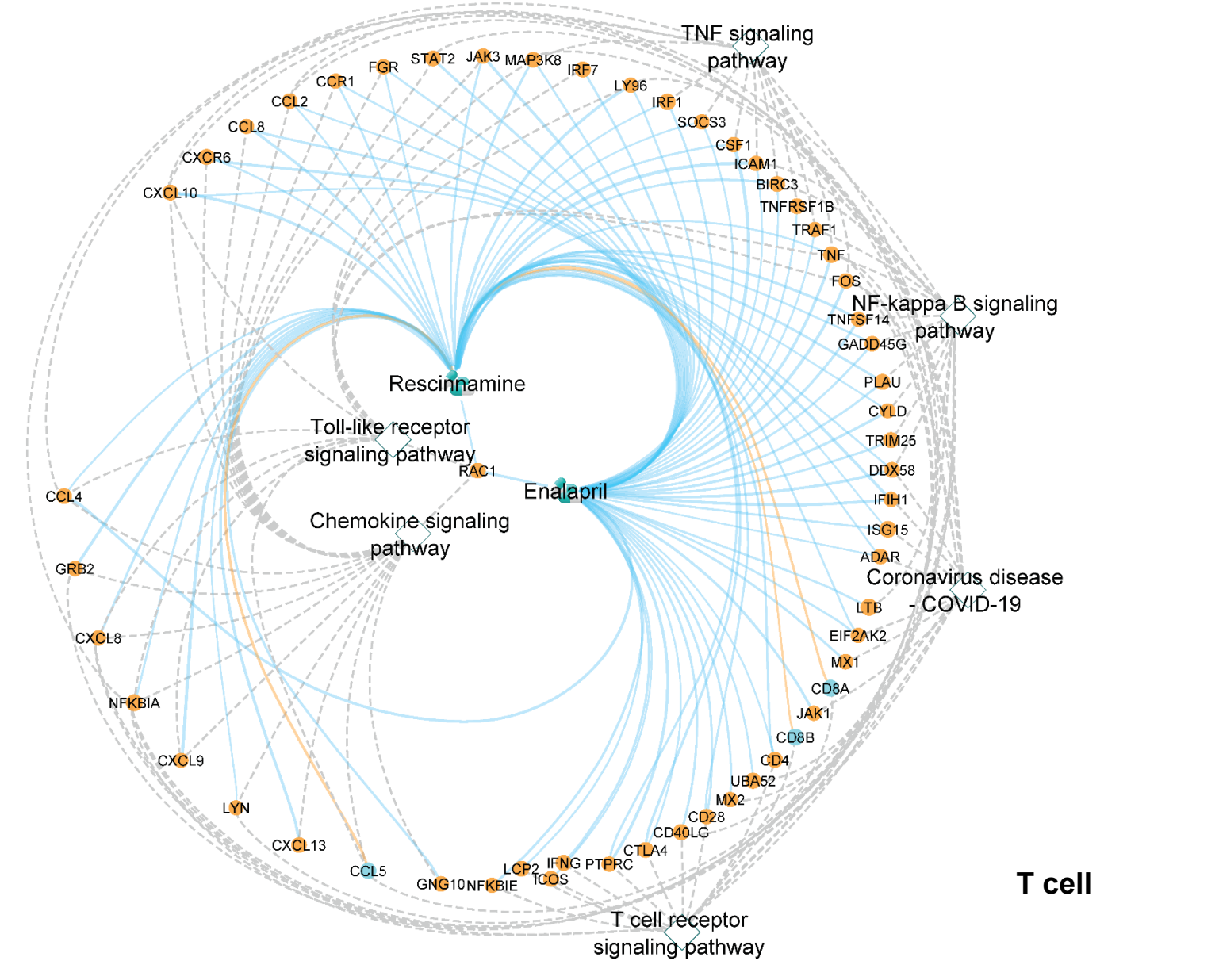
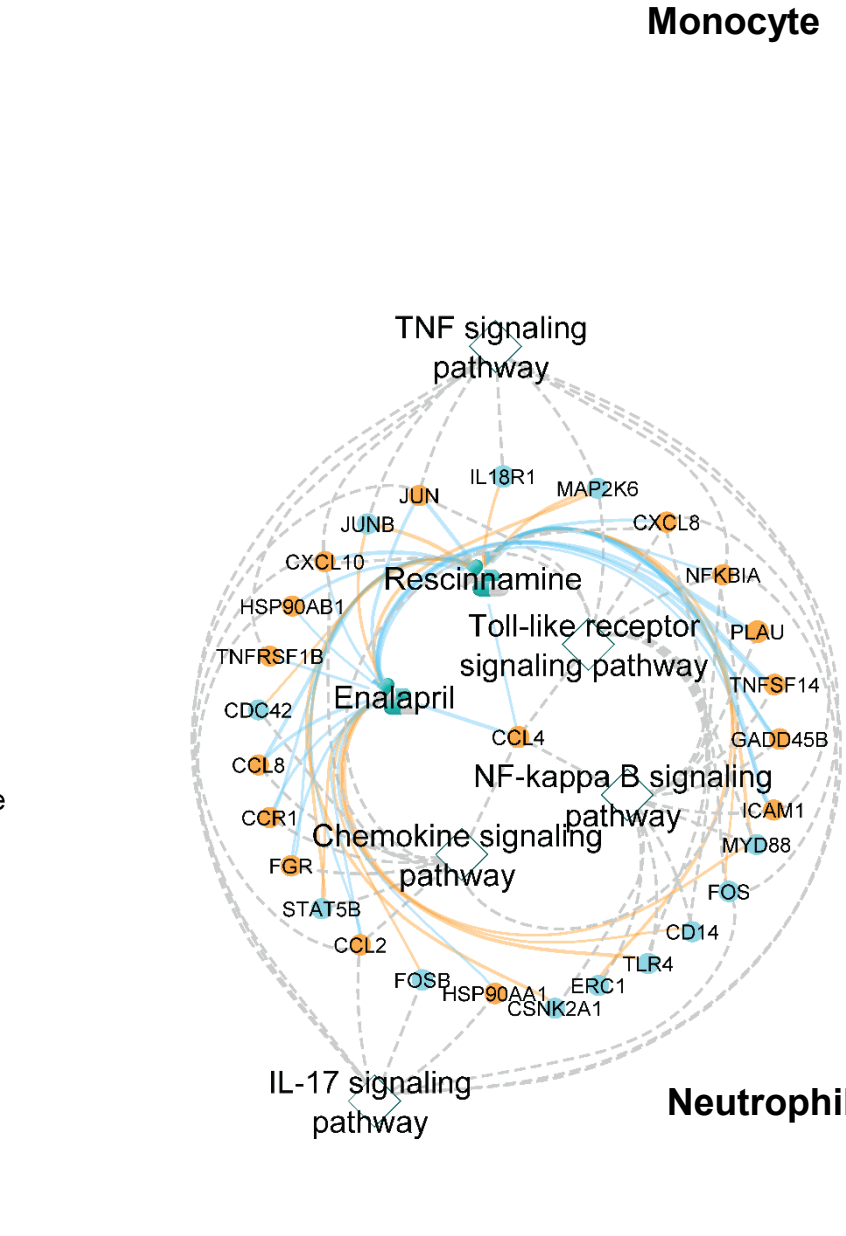
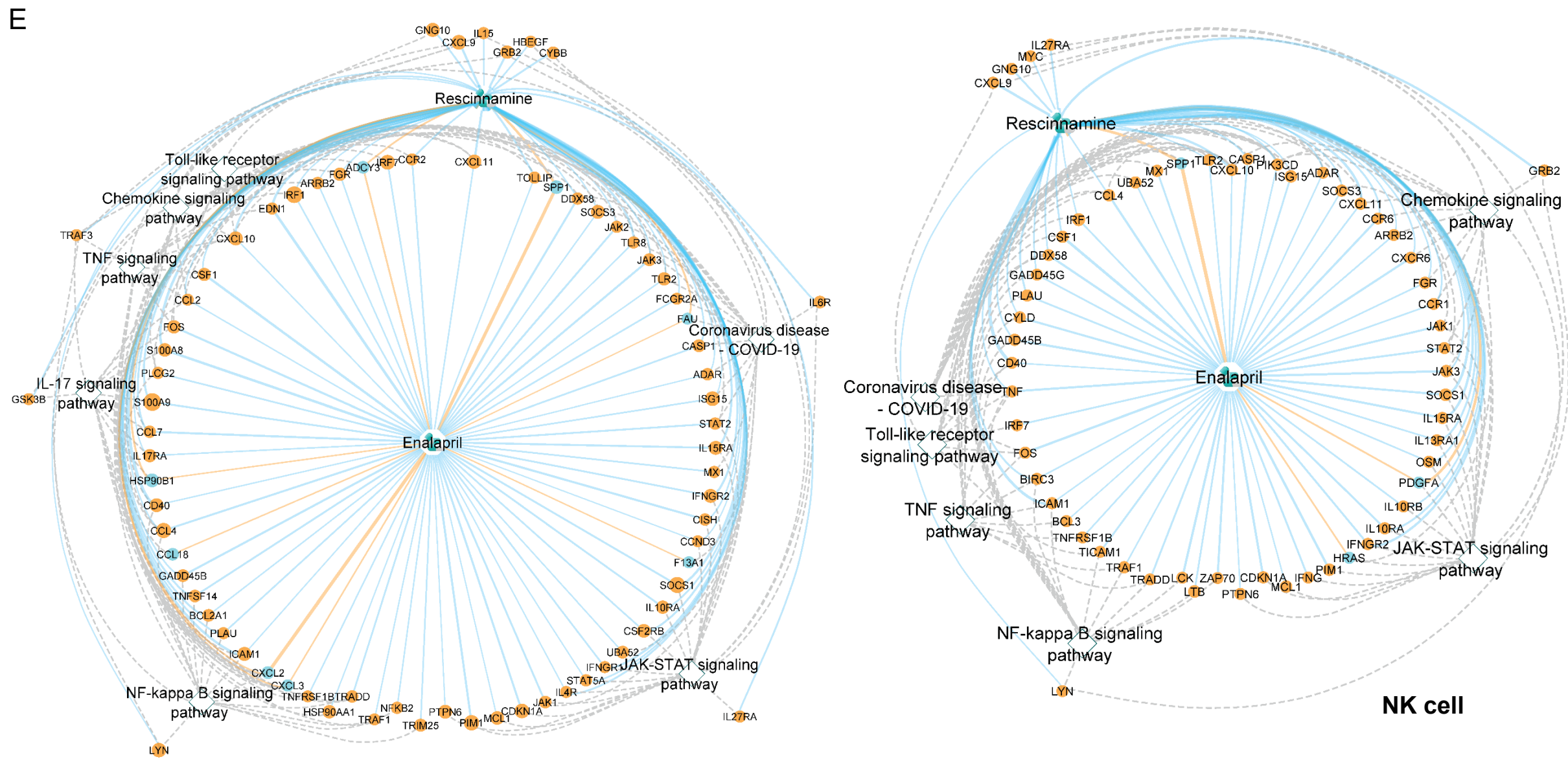
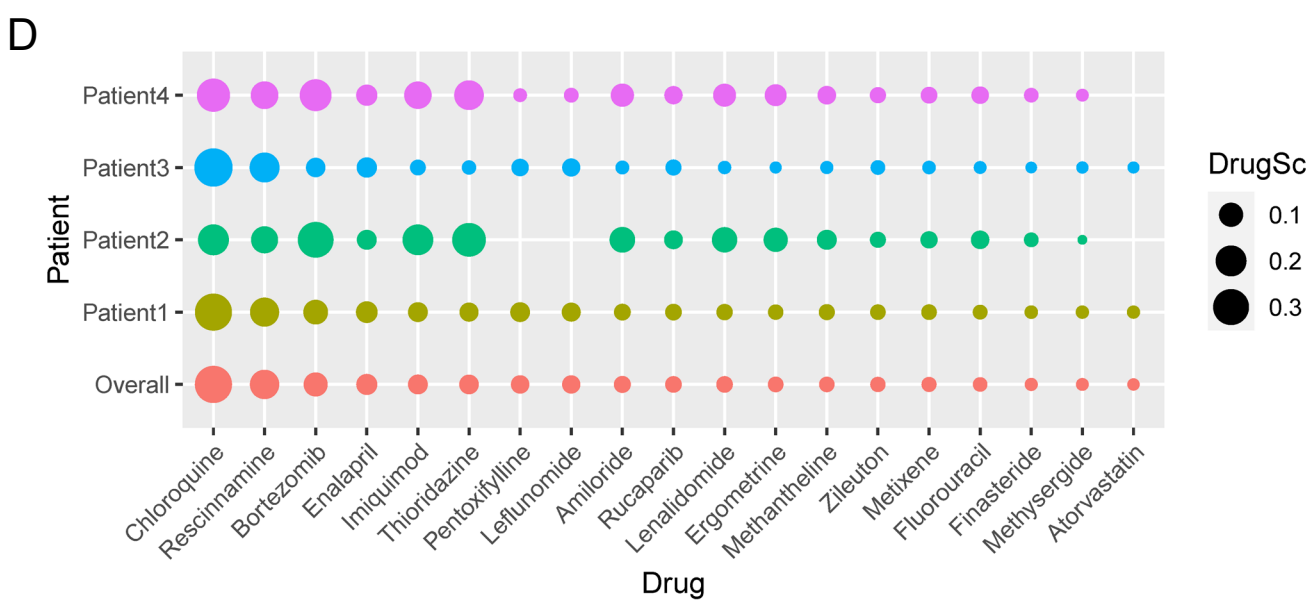
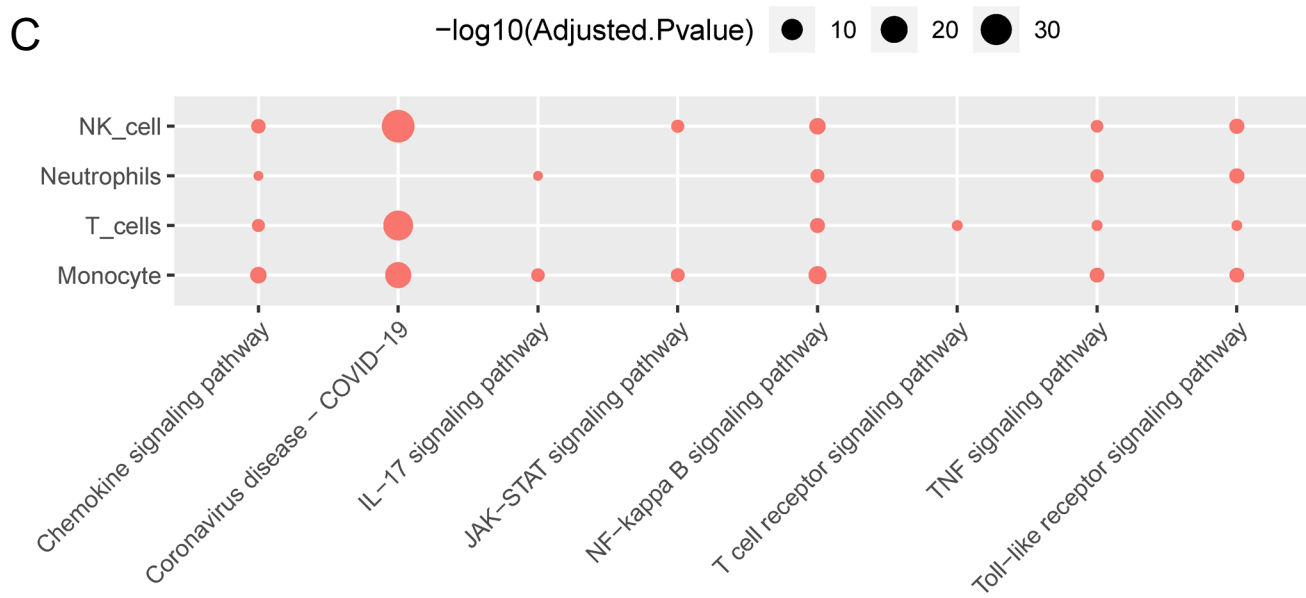
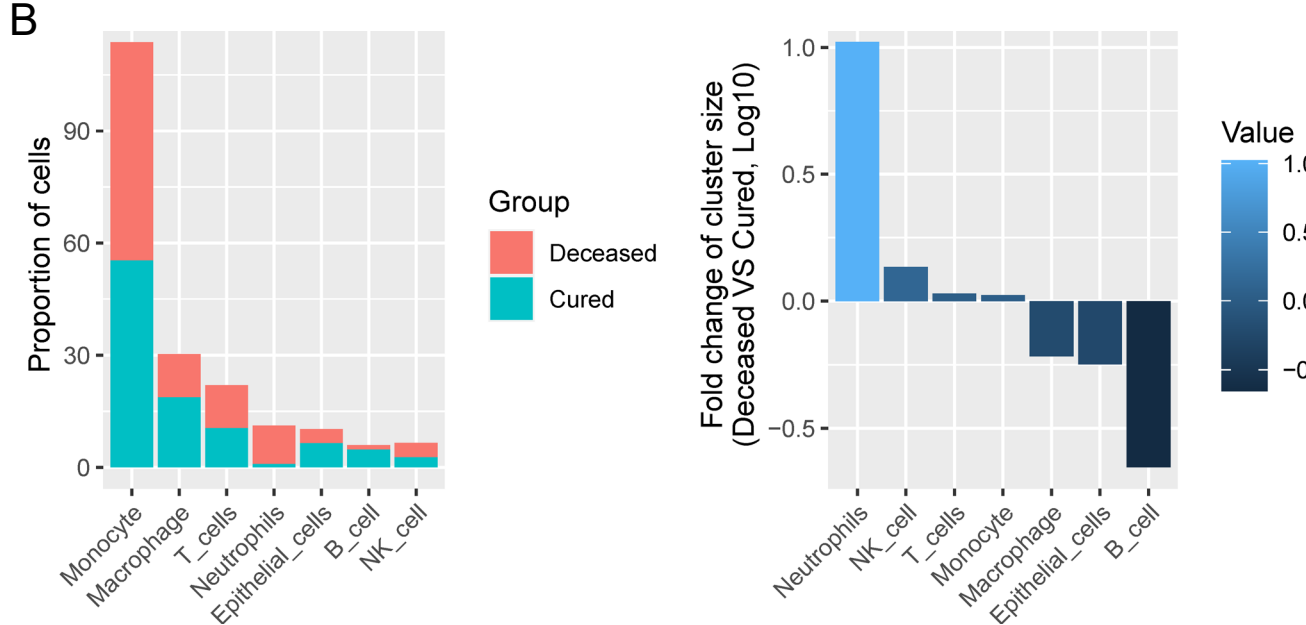
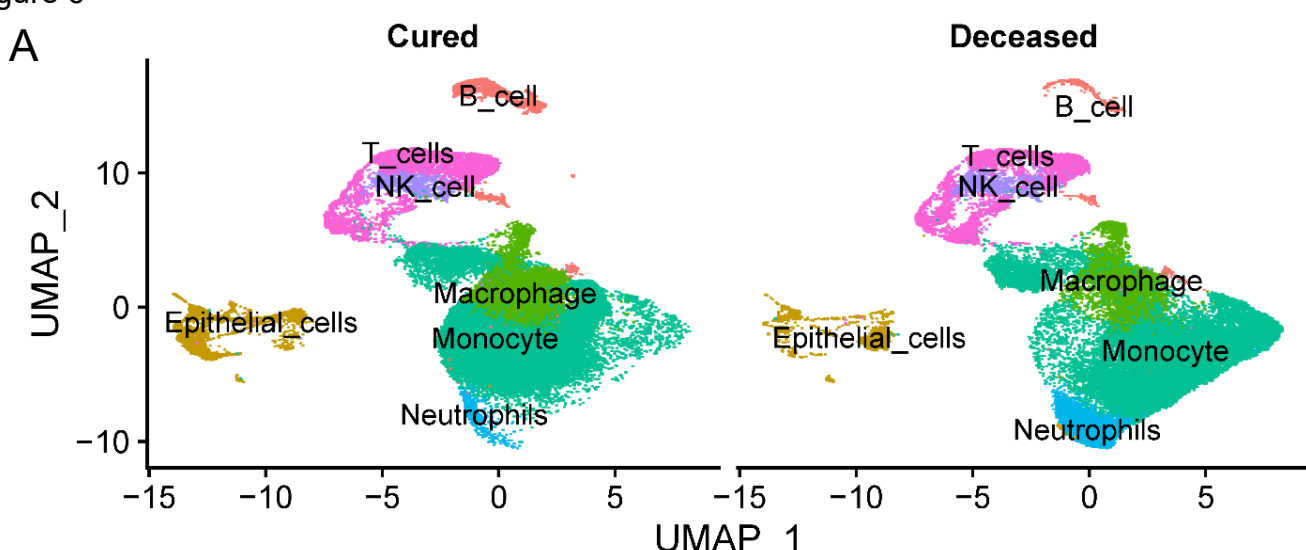


Figure 5





Reference

1. Dagogo-Jack, I. & Shaw, A. T. Tumour heterogeneity and resistance to cancer therapies. *Nat. Rev. Clin. Oncol.* **15**, 81–94 (2018).
2. Devi, G. & Scheltens, P. Heterogeneity of Alzheimer's disease: consequence for drug trials? *Alzheimers. Res. Ther.* **10**, 122 (2018).
3. Caprio, F. Z. & Sorond, F. A. Cerebrovascular Disease: Primary and Secondary Stroke Prevention. *Med. Clin. North Am.* **103**, 295–308 (2019).
4. Sominsky, L., Walker, D. W. & Spencer, S. J. One size does not fit all - Patterns of vulnerability and resilience in the COVID-19 pandemic and why heterogeneity of disease matters. *Brain Behav. Immun.* **87**, 1–3 (2020).
5. Pectasides, E. *et al.* Genomic Heterogeneity as a Barrier to Precision Medicine in Gastroesophageal Adenocarcinoma. *Cancer Discov.* **8**, 37–48 (2018).
6. Molinari, C. *et al.* Heterogeneity in Colorectal Cancer: A Challenge for Personalized Medicine? *Int. J. Mol. Sci.* **19**, (2018).
7. Chen, B. *et al.* Harnessing big 'omics' data and AI for drug discovery in hepatocellular carcinoma. *Nat. Rev. Gastroenterol. Hepatol.* **17**, 238–251 (2020).
8. Heath, J. R., Ribas, A. & Mischel, P. S. Single-cell analysis tools for drug discovery and development. *Nat. Rev. Drug Discov.* **15**, 204–216 (2016).
9. Huang, Q., Liu, Y., Du, Y. & Garmire, L. X. Evaluation of Cell Type Annotation R Packages on Single-cell RNA-seq Data. *Genomics Proteomics Bioinformatics* (2020) doi:10.1016/j.gpb.2020.07.004.
10. Ortega, M. A. *et al.* Using single-cell multiple omics approaches to resolve tumor heterogeneity. *Clin. Transl. Med.* **6**, 46 (2017).
11. Merino, D. *et al.* Barcoding reveals complex clonal behavior in patient-derived xenografts of metastatic triple negative breast cancer. *Nat. Commun.* **10**, 766 (2019).

12. Losic, B. *et al.* Intratumoral heterogeneity and clonal evolution in liver cancer. *Nat. Commun.* **11**, 291 (2020).
13. Liao, M. *et al.* Single-cell landscape of bronchoalveolar immune cells in patients with COVID-19. *Nat. Med.* **26**, 842–844 (2020).
14. Lähnemann, D. *et al.* Eleven grand challenges in single-cell data science. *Genome Biol.* **21**, 31 (2020).
15. Garmire, L. X., Yuan, G.-C., Fan, R., Yeo, G. W. & Quackenbush, J. SINGLE CELL ANALYSIS, WHAT IS IN THE FUTURE? in *Biocomputing 2019* 332–337 (WORLD SCIENTIFIC, 2018).
16. Pushpakom, S. *et al.* Drug repurposing: progress, challenges and recommendations. *Nat. Rev. Drug Discov.* **18**, 41–58 (2019).
17. Alakwaa, F. M. Repurposing Didanosine as a Potential Treatment for COVID-19 Using Single-Cell RNA Sequencing Data. *mSystems* **5**, (2020).
18. Stuart, T. *et al.* Comprehensive Integration of Single-Cell Data. *Cell* **177**, 1888–1902 e21 (2019).
19. Guo, K. *et al.* Identification of Repurposal Drugs and Adverse Drug Reactions for Various Courses of Coronavirus Disease 2019 (COVID-19) Based on Single-cell RNA Sequencing Data. *arXiv* 2005.07856 (2020).
20. He, B. *et al.* Combination therapeutics in complex diseases. *J. Cell. Mol. Med.* **20**, 2231–2240 (2016).
21. Nguyen, Q. H. *et al.* Profiling human breast epithelial cells using single cell RNA sequencing identifies cell diversity. *Nat. Commun.* **9**, 2028 (2018).
22. Aran, D. *et al.* Reference-based analysis of lung single-cell sequencing reveals a transitional profibrotic macrophage. *Nat. Immunol.* **20**, 163–172 (2019).
23. Ritchie, M. E. *et al.* limma powers differential expression analyses for RNA-sequencing and microarray studies. *Nucleic Acids Res.* **43**, e47 (2015).

24. Love, M. I., Huber, W. & Anders, S. Moderated estimation of fold change and dispersion for RNA-seq data with DESeq2. *Genome Biol.* **15**, 550 (2014).
25. McCarthy, D. J., Chen, Y. & Smyth, G. K. Differential expression analysis of multifactor RNA-Seq experiments with respect to biological variation. *Nucleic Acids Res.* **40**, 4288–4297 (2012).
26. Subramanian, A. *et al.* A Next Generation Connectivity Map: L1000 Platform and the First 1,000,000 Profiles. *Cell* **171**, 1437–1452 e17 (2017).
27. Chan, J., Wang, X., Turner, J. A., Baldwin, N. E. & Gu, J. Breaking the paradigm: Dr Insight empowers signature-free, enhanced drug repurposing. *Bioinformatics* **35**, 2818–2826 (2019).
28. Tibshirani, R. & Hastie, T. Outlier sums for differential gene expression analysis. *Biostatistics* **8**, 2–8 (2007).
29. He, B. & Garmire, L. Prediction of repurposed drugs for treating lung injury in COVID-19. *F1000Res.* **9**, 609 (2020).
30. Yoon, S., Baik, B., Park, T. & Nam, D. Powerful p-value combination methods to detect incomplete association. *Sci. Rep.* **11**, 6980 (2021).
31. Wishart, D. S. *et al.* DrugBank 5.0: a major update to the DrugBank database for 2018. *Nucleic Acids Res.* **46**, D1074–D1082 (2018).
32. Kuhn, M., Letunic, I., Jensen, L. J. & Bork, P. The SIDER database of drugs and side effects. *Nucleic Acids Res.* **44**, D1075–9 (2016).
33. Robin, X. *et al.* pROC: an open-source package for R and S+ to analyze and compare ROC curves. *BMC Bioinformatics* **12**, 77 (2011).
34. R Foundation for Statistical Computing, R. C. R: A language and environment for statistical computing. *R Foundation for Statistical Computing* (2016).
35. Caron, M. *et al.* Single-cell analysis of childhood leukemia reveals a link between developmental states and ribosomal protein expression as a source of intra-individual

- heterogeneity. *Sci. Rep.* **10**, 8079 (2020).
36. Ren, X. *et al.* COVID-19 immune features revealed by a large-scale single-cell transcriptome atlas. *Cell* **184**, 1895–1913.e19 (2021).
 37. Corsello, S. M. *et al.* The Drug Repurposing Hub: a next-generation drug library and information resource. *Nat. Med.* **23**, 405–408 (2017).
 38. Ching, T., Huang, S. & Garmire, L. X. Power analysis and sample size estimation for RNA-Seq differential expression. *RNA* **20**, 1684–1696 (2014).
 39. Farooq, M. & Patel, S. P. Fulvestrant. in *StatPearls* (2020).
 40. Neratinib for breast cancer. *Aust Prescr* **42**, 209–210 (2019).
 41. Connell, N. T. & Berliner, N. Fostamatinib for the treatment of chronic immune thrombocytopenia. *Blood* **133**, 2027–2030 (2019).
 42. Johnson, L. *et al.* Novel Colchicine Derivatives and their Anti-cancer Activity. *Curr. Top. Med. Chem.* **17**, 2538–2558 (2017).
 43. Bower, J. J. *et al.* Patterns of cell cycle checkpoint deregulation associated with intrinsic molecular subtypes of human breast cancer cells. *NPJ Breast Cancer* **3**, 9 (2017).
 44. Wong, W. M. Tretinoin in the treatment of acute promyelocytic leukemia. *Cancer Pract.* **4**, 220–223 (1996).
 45. Prebet, T. & Vey, N. Vorinostat in acute myeloid leukemia and myelodysplastic syndromes. *Expert Opin. Investig. Drugs* **20**, 287–295 (2011).
 46. Sawai, C. M. *et al.* Therapeutic targeting of the cyclin D3:CDK4/6 complex in T cell leukemia. *Cancer Cell* **22**, 452–465 (2012).
 47. Nagata, K., Ohtani, K., Nakamura, M. & Sugamura, K. Activation of endogenous c-fos proto-oncogene expression by human T-cell leukemia virus type I-encoded p40tax protein in the human T-cell line, Jurkat. *J. Virol.* **63**, 3220–3226 (1989).
 48. Raetz, E. A. & Teachey, D. T. T-cell acute lymphoblastic leukemia. *Hematology Am. Soc. Hematol. Educ. Program* **2016**, 580–588 (2016).

49. Bao, C. *et al.* Natural killer cells associated with SARS-CoV-2 viral RNA shedding, antibody response and mortality in COVID-19 patients. *Exp. Hematol. Oncol.* **10**, 5 (2021).
50. Vanderbeke, L. *et al.* Monocyte-driven atypical cytokine storm and aberrant neutrophil activation as key mediators of COVID-19 disease severity. *Nat. Commun.* **12**, 4117 (2021).
51. Swadling, L. & Maini, M. K. T cells in COVID-19 - united in diversity. *Nature immunology* vol. 21 1307–1308 (2020).
52. Ondracek, A. S. & Lang, I. M. Neutrophil Extracellular Traps as Prognostic Markers in COVID-19: A Welcome Piece to the Puzzle. *Arteriosclerosis, thrombosis, and vascular biology* vol. 41 995–998 (2021).
53. Zhu, X., Ching, T., Pan, X., Weissman, S. M. & Garmire, L. Detecting heterogeneity in single-cell RNA-Seq data by non-negative matrix factorization. *PeerJ* **5**, e2888 (2017).
54. Cherry, C. *et al.* Intercellular signaling dynamics from a single cell atlas of the biomaterials response. *bioRxiv* 2020.07.24.218537 (2020) doi:10.1101/2020.07.24.218537.
55. He, B. *et al.* Drug discovery in traditional Chinese medicine: from herbal fufang to combinatory drugs. *Science* (2015).
56. Le Du, F., Diéras, V. & Curigliano, G. The role of tyrosine kinase inhibitors in the treatment of HER2+ metastatic breast cancer. *Eur. J. Cancer* **154**, 175–189 (2021).
57. Yang, X., Wu, D. & Yuan, S. Tyrosine Kinase Inhibitors in the Combination Therapy of HER2 Positive Breast Cancer. *Technol. Cancer Res. Treat.* **19**, 1533033820962140 (2020).
58. Kuiatse, I. *et al.* Targeting the Spleen Tyrosine Kinase with Fostamatinib as a Strategy against Waldenström Macroglobulinemia. *Clin. Cancer Res.* **21**, 2538–2545 (2015).
59. Taylor, E. W. THE MECHANISM OF COLCHICINE INHIBITION OF MITOSIS. I. KINETICS OF INHIBITION AND THE BINDING OF H³-COLCHICINE. *J. Cell Biol.* **25**, SUPPL:145–60 (1965).
60. Thu, K. L., Soria-Bretones, I., Mak, T. W. & Cescon, D. W. Targeting the cell cycle in breast cancer: towards the next phase. *Cell Cycle* **17**, 1871–1885 (2018).

61. Kalil, A. C. *et al.* Baricitinib plus Remdesivir for Hospitalized Adults with Covid-19. *N. Engl. J. Med.* **384**, 795–807 (2021).
62. Hippisley-Cox, J. *et al.* Risk of severe COVID-19 disease with ACE inhibitors and angiotensin receptor blockers: cohort study including 8.3 million people. *Heart* **106**, 1503–1511 (2020).
63. Derington, C. G. *et al.* Angiotensin II receptor blocker or angiotensin-converting enzyme inhibitor use and COVID-19-related outcomes among US Veterans. *PLoS One* **16**, e0248080 (2021).
64. Del Valle, D. M. *et al.* An inflammatory cytokine signature predicts COVID-19 severity and survival. *Nat. Med.* **26**, 1636–1643 (2020).